Results in Engineering 26 (2025) 105008

Contents lists available at ScienceDirect

Results in Engineering

journal homepage: www.sciencedirect.com/journal/results-in-engineering

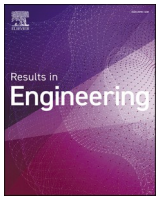

Research paper

Enhancement of dicoumarol production by *Aspergillus fumigatus* using methanolic extract of *Gliricidia sepium* leaves: Insights into fermentation kinetics parameters

Siti Zalina Yaacob [a], Luqman Chuah Abdullah [a,b,c,*], Chuan Li Lee [b,*], Nor Hafizah Abdullah [a], Kit Ling Chin [c]

[a] Department of Chemical and Environmental Engineering, Faculty of Engineering, Universiti Putra Malaysia, 43400 UPM Serdang, Selangor, Malaysia
[b] Bioprocessing and Biomanufacturing Research Complex, Faculty of Biotechnology and Biomolecular Sciences, Universiti Putra Malaysia, 43400 UPM Serdang, Selangor, Malaysia
[c] Institute of Tropical Forestry and Forest Products, Universiti Putra Malaysia, 43400 UPM Serdang, Selangor, Malaysia

ARTICLE INFO

Keywords:
Gliricidia sepium
O-coumaric acid
Aspergillus fumigatus
Fermentation
Initial concentration of glucose
Initial concentration of nitrogen

ABSTRACT

The bioconversion of dicoumarol by *Aspergillus fumigatus* NRRL 163 using methanolic extract of *Gliricidia sepium* leaves was thoroughly investigated, special emphasis on the influence of medium composition and fermentation conditions. The ideal conditions were determined by utilizing a defined medium containing o-coumaric acid extracted from *G.sepium* leaves. This resulted in the highest dicoumarol productivity (153.81 U mL h^{-1}), cell efficiency (0.027 g L $cell^{-1}$), and overall dicoumarol productivity (4.15 U mL·h^{-1}). The Monod kinetic model effectively described the relationship between growth rate, substrate concentration, and biomass production. With over 95 % confidence, the model showed no significant difference between calculated and observed values, confirming its accuracy in predicting microbial growth, substrate utilization, and dicoumarol biosynthesis. This approach enhanced dicoumarol productivity (167.92 U mL^{-1} h^{-1}) and cell efficiency (37.13 g mL^{-1} $cells^{-1}$). Furthermore, an extensive quantitative analysis utilizing HPLC, FTIR, LCMS/MS and vitro rodenticides (aPTT and PT test) was conducted, revealing substantial anticoagulant activity of dicoumarol, notably in inhibiting intrinsic pathways of coagulation. The successful identification of dicoumarol through LCMS/MS and the confirmation of its structure ($C_{19}H_{12}O_6$) via FT-IR spectra highlighted the robustness of the approach. Moreover, the dicoumarol fraction's ability to double coagulation time in the aPTT test underscored its potent anticoagulant properties. These findings offer novel insights into dicoumarol bioconversion and its pharmacological significance in rodenticide anticoagulant activity.

1. Introduction

Dicoumarol, commonly referred to as bis-hydroxycoumarin, exemplifies the advantages of integrating western and traditional medicines [1]. Known for its anticoagulant and anti-inflammatory properties, dicoumarol is also recognized for its significant bioactive effects [2,3]. For example, dicoumarol can clinically prevent and treat thrombosis and thrombophlebitis, and can treat various thromboembolic diseases. Dicoumarol is an oral medication that shares the same anticoagulant mechanism as warfarin. It has also been documented to possess other biological activities, including anticancer, antimicrobial, and antiviral effects. Lately, computational screening identified dicoumarol, a natural anticoagulant, as a potential inhibitor of SARS-CoV-2. However, its inhibitory effects and potential mechanisms of action remain to be fully understood [4].

Derived from plants, dicoumarol is a naturally occurring chemical that has been thoroughly investigated as a natural anticoagulant medication owing to its potential application in pharmaceutical research [5]. Both natural and synthetic dicoumarols have been established as effective anticoagulant drugs in medical applications. Dicoumarol was discovered in numerous plants like *Melilotus officinalis (L.) Pall* [3], *Gerbera anandria* [6], *G. sepium* [7] and others. All of these plants have characteristics comparable in that they contain a high quantity of coumarin, which can be converted to dicoumarol, which has been shown

* Corresponding authors.
E-mail addresses: chuah@upm.edu.my (L.C. Abdullah), chuanli@upm.edu.my (C.L. Lee).

https://doi.org/10.1016/j.rineng.2025.105008
Received 27 February 2025; Received in revised form 10 April 2025; Accepted 19 April 2025
Available online 21 April 2025

to have a wide spectrum of antitumor and antibacterial activity in vitro and in vivo and is being evaluated as a potential novel cancer chemoprevention drug [8].

Several studies have shown that microbial enzymes can efficiently catalyze the production of dicoumarols from o-coumaric acid [1,9]. Notably, a plant with the ability to produce both o-coumaric acid and dicoumarol would offer dual benefits, thus enhancing its potential. It has been reported by Takemura et al. [10], *G. sepium* leaf tissue is found to contain both coumarin and o-coumaric acid. Moreover, *G. sepium* demonstrates a diverse array of pharmacological properties, encompassing cytotoxic, antimicrobial, antibacterial, anti-inflammatory, antioxidant, thrombolytic, antisickling, wound healing, larvicidal, and anthelmintic actions [11]. Despite the well-known therapeutic potential of dicoumarol, studies exploring its microbial bioconversion using naturally derived o-coumaric acid from *G.sepium* remain limited. This study fills the gap by presenting a novel biotechnological approach for dicoumarol synthesis, integrating plant biochemistry with microbial catalysis.

In light of this, *G. sepium* represents a promising prospect, not only for its capacity to produce both o-coumaric acid and dicoumarol, but also due to its widespread growth across arid regions beyond its native range, where it supports the cultivation of crops such as cocoa. The abundance of its lignocellulosic biomass especially *G. sepium*'s leaves the offers a valuable opportunity for sustainable bioenergy and biofuel production [12]. These attributes highlight the importance of further exploration into its bioconversion potential. Bioconversion of dicoumarol presents a promising alternative within the realm of green technologies, offering efficiency and cost-effectiveness. Fermentation, among other bioconversion processes has a mild reaction conditions, is more sustainable and convenient to be achieved compared to conventional chemical synthesis [9]. Their capacity for dicoumarol production emphasizes the significance of exploring their bioconversion capabilities further. Recent research highlights the economic and social benefits of bio-based innovations, particularly in developing regions where eco-friendly technologies support rural development and public health [13]. Additionally, biotechnological applications like dicoumarol-based anticoagulants align with goals to reduce synthetic chemicals and promote biological alternatives [14]. The growing focus on sustainable biotechnology further strengthens the relevance of this study.

Among various microbial species, *Aspergillus fumigatus* has demonstrated significant potential in a wide range of bioconversion applications due to its robust metabolic pathways and ability to produce bioactive compounds [15–17]. This species is known for its fast growth rate and resilience, which makes it an excellent choice for industrial biotechnological processes. *A. fumigatus* can thrive under diverse environmental conditions, making it adaptable to different fermentation environments [18]. Furthermore, the species has shown promise in producing a variety of bioactive molecules, including antimicrobial and anticancer compounds [19], which highlights its versatility beyond dicoumarol production. The ability of *A. fumigatus* to metabolize various substrates, including plant-based compounds, provides an added advantage for bioconversion processes like the production of value-added chemicals, enzymes, and natural products. The flexibility of *A. fumigatus* in utilizing different carbon and nitrogen sources makes it a reliable organism for large-scale fermentation processes [20]. Although *A. fumigatus* has been extensively studied, its potential for the bioconversion of specific plant-derived substrates, such as *G. sepium* leaves, remains underexplored. By using *A. fumigatus* for this novel conversion process, the present research aims to address this unexplored area.

The bioconversion approach utilizing *A. fumigatus* is employed in this research, with the primary focus on a fermentation process for converting o-coumaric acid extracted from *G.sepium* leaves into dicoumarol. This process, conducted using a shake flask, aims to enhance the activity of dicoumarol as a rodenticide anticoagulant. The research also explores various enhancement strategies and potential applications of dicoumarol bioconversion, specifically emphasizing the unique attributes *of A. fumigatus Fresenius* NRRL 163 in improving rodenticide anticoagulant activity. To investigate the fermentation yield in the shake flask system, a one-factor-at-a-time approach (OFAT) was employed to evaluate the effects of media composition, initial concentration of glucose, and initial concentration of nitrogen on *A. fumigatus* growth and dicoumarol production. This method was selected for its simplicity and effectiveness in providing clear insights into how each factor influences the fermentation process. By varying one parameter at a time, the approach enables precise identification of the conditions that enhance the bioconversion of o-coumaric acid into dicoumarol. Drawing from its successful application in enzyme production optimization [21] and erythritol production enhancement [22], the OFAT approach has proven to be a reliable strategy for improving fermentation outcomes. It simplifies experimental design while allowing careful evaluation of each factor's impact, particularly beneficial during the early stages of process development. The data derived from this method will contribute to identifying the ideal conditions for maximizing dicoumarol production in *A. fumigatus*, supporting the development of efficient bioconversion processes.

Apart from that, microorganisms exhibit varying growth rates in different environments, influenced by physiological activities. Fermentation kinetic is crucial as it defined the growth and product formation during active cell growth, as well as during the activities of resting and dying cells. Moreover, kinetic modeling is essential for developing fermentation processes, as it facilitates determining ideal operational conditions for target metabolite production. In order to create kinetic parameter values that would serve as the foundation for a kinetic model of the process, experimental data from the batch fermentation of *A. fumigatus* Fresenius NRRL 163 generating dicoumarol were investigated throughout the present research. Through comprehensive investigation and analysis, our research aims to shed light on the efficient and cost-effective utilization of dicoumarol in pest management practices, contributing to advancements in sustainable agricultural practices.

2. Material and methods

2.1. Plant material and experimental setup

2.1.1. Extraction of o-coumaric acid from the leaves of G. sepium

The leaves of *G. sepium* were collected from various local residential areas in Nilai, Negeri and were oven-dried at 50°C until constant weight. The oven-dried *G. sepium* leaf samples were used for the extraction of o-coumaric acid using methanol as the solvent with ultrasonic-assisted extraction method. The extraction method involved immersing the ultrasound probe in the mixture containing 80 % of methanol and *G. sepium* leaf samples with solvent-to-solid ratio of 10:1 mg L^{-1}. The mixture was heated in a water bath at 46.6°C for 45 min, with an ultrasound probe operating at a constant power of 130 W and a frequency of 20 kHz. Subsequently, the leaf extract containing o-coumaric acid was filtered using Whatman No. 1 filter paper, and the filtrate was evaporated to obtain a dry extract by air drying at room temperature under a hood for 24 h. The dry extract from *G. sepium* leaves containing 42.4 mg/kg of o-coumaric acid.

2.1.2. Bioconversion of o-coumaric acid to dicoumarol using shake flask fermentation A. fumigatus inoculum preparation

An inoculum containing *Aspergillus fumigatus* Fresenius NRRL 163 was prepared. Stock cultures were streaked on potato dextrose agar (PDA) and incubated at 37°C overnight. A single colony was removed from PDA and inoculated into 100 mL of potato dextrose broth in Erlenmeyer flasks (500 mL). Inoculated flasks were shaken vigorously (rotary shaker, 200 rev per min) for 10 – 12 h at 37°C. The cell viability was tested and cell count was done using haemocytometer. The inoculum with minimum 1.0×10^6 CFU/mL was used as a standard inoculum for fermentation in shake flasks.

2.1.3. Evaluation of fermentation conditions for dicoumarol production

The fermentation conditions were determined by studying the effect of various parameters, including the type of medium composition, initial concentration of glucose and nitrogen on the highest yield of dicoumarol. One-factor-at-a-time (OFAT) approach is effective when factors behave independently, providing a straightforward and cost-effective solution. It provides additional benefits by arranging experimental factors for their expected size and main effect into the factorial design [23]. In this present research, the OFAT approach was applied and divided into three stages.

In the first stage, the selection of medium composition; complex medium and defined medium were conducted in batch fermentation using shake flask culture. Two types of fermentation medium were used to evaluate the effect of different medium on the yield of dicoumarol:

I. Defined medium. The fermentation medium consists of dry extract from *G. sepium* leaves (5g), D-glucose (5g), $NaNO_3$ (5g), KCI (0.52g), $MgSO_4.7H_2O$ (0.59g), KH_2PO_4 (1.52g) and trace elements of $FeSO_4.7H_2O$ (4mg), $ZnSO_4.7H_2O$ (0.4mg) was added into 1L deionized water.

II. Complex medium. The fermentation medium consists 5g of *G. sepium* dry extract containing o-coumaric acid (5g) and 24 g L^{-1} of potato dextrose broth (OXOID Thermo Fisher Scientific).

Submerged fermentation was conducted in 500 mL flasks with 200mL working volume. 20 mL of inoculum containing minimum of 1.0×10^6 spores/mL were inoculated into each flask containing 180 mL of fermentation medium. Inoculated flasks were incubated at 30 °C and 250 rpm. Regular sampling was done at defined time intervals for viability test and biomass determination.

Fermentation medium (defined medium or complex medium) that produced the highest dicoumarol was selected and set as the fermentation parameter for further testing on the bioconversion of o-coumaric acid to dicoumarol in the second stage; effect of initial concentration of glucose, and in the third stage; effect of initial concentration of nitrogen. The effect of initial concentration of glucose (0, 5, 10, 15, 20, 25 g/L) was evaluated and the concentration that resulted with the highest yield was selected to be used in the final stage for the evaluation of initial concentration of nitrogen (0, 1, 2, 3, 4, 5 g/L). Using one-factor-at-a-time approach, type of medium composition, concentration of initial concentration of glucose and nitrogen which produced the highest yield of dicoumarol were recorded. Additionally, the fermentation data /kinetics parameters included the maximum specific growth rate (μ_{max}), biomass yield ($Y_{x/s}$), product yield ($Y_{p/s}$) and growth associated constant (α) were determined.

2.2. Mathematical model formulation of growth and dicoumarol production of A. fumigatus

Understanding the kinetics of microbial growth, substrate utilization, identification of limiting nutrients affecting cell growth, and determining endogenous decay rates are crucial for effective growth control and maintaining biomass balance within the system [24,25]. The yield coefficient and the specific growth rate were utilized to develop the Monod microbial growth kinetic model.

2.2.1. Monod kinetics for microbial growth

The Monod model is an unstructured model that is dependent on substrate concentration. It is widely used to describe the specific growth rate, (μ) of microbial cells as a function of a limiting or low substrate concentration [26,27]. This model was applied to describe the growth of *A. fumigatus* based on substrate-limited kinetics, and it has been proven to be sufficient to accurately capture the microbial growth dynamics under the given experimental conditions. Numerous studies have shown the model's robustness and reliability in accurately predicting microbial growth in substrate-limited environments, particularly in systems where the substrate concentration is the primary limiting factor [28]. This makes the Monod model an effective tool for understanding microbial growth dynamics in similar settings.

2.2.1.1. Specific growth rate. The specific growth rate (μ) of the microorganism is a function of the substrate concentration (S) and can be described by the Monod equation:

$$\mu = \mu\max\left(\frac{S}{S+Ks}\right) \tag{1}$$

Where;

μ_{max} = maximum specific growth rate (h^{-1})
S = substrate concentration (g/L)
K_s = Monod saturation constant (g/L)

Eq. 2 is further simplified as;

$$\frac{1}{\mu} = \frac{Ks}{\mu\max(S)} + \frac{1}{\mu max} \tag{2}$$

Multiplying both side equation with S then;

$$S{\cdot}\mu = Ks{\cdot}\mu\max + \frac{S}{\mu max} \tag{3}$$

2.2.1.2. Yield coefficient (Y)

$$Y = \frac{\mathrm{dX}}{dS} \tag{4}$$

Where;

dX = mass of new cells
dS = mass of substrate consumed

The yield coefficient, commonly referred to as the substrate-to-biomass yield, is used to convert between biomass growth rate $\frac{dX}{dt}$ and substrate utilization rate $\frac{dS}{dt}$.

Where;

X_0 = initial biomass concentration (mg/mL)
X = biomass concentration (mg/L)
t = incubation time (h)

2.2.1.3. Biomass growth rate, $\frac{dX}{dt}$. By rearranging the Monod equation (Eq. 1) and Eq. 3, the expression for the time-rate of biomass change can be obtained as:

$$\frac{dX}{dt} = \mu Xo = \mu\max Xo\left(\frac{S}{S+Ks}\right) \tag{5}$$

2.2.1.4. Substrate utilization rate, $\frac{dS}{dt}$. Similarly, by combining the expressions for the yield coefficient (Eq. 4) and the Monod equation (Eq. 2), an expression for the substrate utilization rate is derived as:

$$\frac{dS}{dt} = \mu XoY\left(\frac{S}{S+Ks}\right) \tag{6}$$

2.2.2. Model fitting to experimental data

The experimental data were fitted to the growth equations using SigmaPlot® computer software via nonlinear regression with the Marquadt algorithm. The model parameter values were initially determined by solving the equations, and the computer program was utilized as a search strategy to minimize the sum of squares of the predicted and measured values. The projected values were then utilized to replicate the cell, substrate, and product concentration profiles throughout

fermentation.

2.3. Statistical analysis

The statistical software SPSS for Windows, version 16.0 (SPSS Inc., Chicago), was used for all analyses. To assess the effects of initial concentration of glucose and nitrogen on dicoumarol production kinetics, a one-way analysis of variance (ANOVA) was conducted at a significance level of 95 % ($p \leq 0.05$). The data were collected from 5 independent biological replicates to ensure robustness and reproducibility. A one-way ANOVA followed by Tukey's post hoc test was applied to identify significant differences between the groups when the ANOVA indicated a significant result ($p \leq 0.05$). Effects with a p-value greater than 0.05 were considered not statistically significant [29].

2.4. Identification and characterisation of dicoumarol

The fermentation broth was incubated on orbital shaker for 72 h. 5 mL of fermentation broth were filtered through a 11μm filter paper (Whatman^{TM} 1001-125 Grade 1, US) to ensure they were free of mycelial debris and then mechanically shaken with an equal volume of chloroform for 20 min. The chloroform layer was then separated and evaporated to about l mL for further dicoumarol analysis using High performance liquid chromatography (HPLC), Fourier Transform Infrared Spectroscopy (FTIR) and Liquid Chromatography-Mass Spectrometry (LCMS/MS).

2.4.1. HPLC analysis

High performance liquid chromatography (Shimadzu, Model SPD 20A, US) was used to analyse the product qualitatively and quantitatively. A ZORBAX Eclipse Plus C18 (4.6 × 250 mm) column was used as stationary phase. The standard of dicoumarol was purchased from Sigma Aldrich (USA). The selected mobile phase combination was chosen to enhance separation, with dicoumarol detection established at 303 nm, as referenced in [28,30]. The gradient elution was performed using the mobile phase consisted of methanol and sodium acetate (75:25 v/v) at pH 6.0. The samples subjected to HPLC analysis included the dicoumarol standard, o-coumaric acid standard, and sample fractions of dicoumarol in both defined and complex medium.

2.4.2. FTIR analysis

A chemical structure by means of presence of functional groups in the samples were identified using FTIR (Model NICOLET Nexus 470, USA) technique with an attenuated total reflectance (ATR) mode in the range between 4000 tom 8000 cm^{-1} averaging 64 scans at a resolution of 8 cm^{-1} was operated for sample analysis.

2.4.3. LCMS/MS analysis

The analysis was performed using liquid chromatography-mass spectrometry (LC-MS/MS) with an ion-trap mass spectrometer featuring an electrospray ionization (ESI) source. This was coupled to an Agilent HPLC system, which included a UV detector, binary gradient pumps, a C-18 column (4.0×250 mm I.D, 1.8 μm particle size, Agilent Technology), a column oven, and a sample auto-injector, all controlled via Chemstation software.

2.5. In vitro rodenticides anticoagulant activity

2.5.1. Plasma collection and processing

Five male adult white rats (Sprague Dawley) at age of 1-2 months were collected from Animal Resource Unit (ARU), Department of Veterinary Pathology and Microbiology, UPM. All the blood collection works were attended by a certified veterinarian with animal ethic permission (practicing certificate number AM18-000035-OC). The rats were brought to the lab in specific cage and their respective body weights were recorded. Blood specimens were collected through venipuncture method and withdrawn in 3.2 % sodium citrate tubes with a collection ratio of (3:1, 5:1, 7:1 and 9:1 blood to anticoagulant). The sodium citrate tubes were filled completely and the specimens were gently mixed after collection. All the specimens were brought to the lab within 4-8 h and kept at 15-25°C to prevent blood haemolysis. The specimens were then capped centrifuged at 3000 rpm for 10 min using Centrifuge (Model Hettich EBA 20, US) to achieve platelet-poor plasma.

Table 1
Comparative study of the kinetic parameter values and the production performance of dicoumarol by *A. fumigatus* in a shake flask using two different types of medium.

Kinetic Parameter Values	Types of Medium	
	Complex Medium	Defined Medium
Maximum specific growth rate, μ_{max} (h^{-1})	0.25	0.12
Maximum biomass concentration, X_{max} (g L^{-1})	10.21	9.33
Maximum dicoumarol concentration, P_{max} (U L^{-1})	0.214	0.322
Cell efficiency, P_{max}/X_{max} (U g $cells^{-1}$)	0.021	0.035
Cell yield, $Y_{x/s}$ (g cells glucose $^{-1}$)	1.18	0.95
Overall biomass productivity, P_x (g L h^{-1})	0.13	0.12
Time to reach maximum dicoumarol production (h)	110	110

2.5.2. Prothrombin time (PT) test

The action in the extrinsic pathway of dicoumarol was evaluated using the PT test [31], conducted with commercial PT reagent kits. Plasma (90 μL) was mixed with 10 μL of anticoagulant samples (sample was prepared under the conditions that produced the maximum yield) (0.1 – 2 μg/μL) and incubated at 37°C for 5 min. Then, 200 μL of PT assay reagent (sodium chloride) pre-warmed at 37°C for 10 min was added and the clotting time was recorded by a digital coagulometer (Pioway, Model CL-2000, China). Plasma alone was used as control (absence of anticoagulant activity). Dicoumarol (1 μg/μL) (Sigma Aldrich (USA)) was used as positive control.

2.5.3. Activated partial thromboplastin (aPTT) test

The action in intrinsic and common pathways of dicoumarol were evaluated by aPTT test [32]. The test was carried out using commercial aPPT reagent kits. Plasma (90 μL) was mixed with 10 μL of anticoagulant samples (sample was prepared under the conditions that produced the maximum yield) (0.1 – 2 μg/μL) and incubated at 37°C for 5 min, before the addition of pre-warmed aPTT reagent (calcium chloride)) and incubation at 37°C for 2 min. Pre-warmed (37°C) 25 mM calcium chloride was then added and the clotting time recorded by a digital coagulometer (Pioway, Model CL-2000, China). Plasma alone was used as control (absence of anticoagulant activity). Dicoumarol (1 μg/μL) (Sigma Aldrich (USA)) was used as positive control.

3. Results and discussion

3.1. Effect of complex and defined media on the dicoumarol production

The performance and kinetic parameter values during fermentation of *A. fumigatus* using different media was depicted in Table 1.

The kinetic parameter values presented in Table 1 offer valuable insights into the influence of medium composition on microbial growth and dicoumarol production. Firstly, the significantly higher maximum specific growth rate observed in the complex medium compared to the defined medium indicates that the former provides a more favorable environment for microbial proliferation, likely due to its richer nutrient composition essential for fungal growth, making them an excellent component of media [33,34]. This disparity is further reflected in the higher maximum biomass concentration achieved in the complex medium, suggesting superior support for microbial growth and biomass

Table 2
Effect of initial concentration of glucose on dicoumarol production and kinetic parameters in submerged cultures of *A. fumigatus*.

Kinetic Parameters	Initial Concentration of Glucose (g L^{-1})						p-value
	0	5	10	15	20	25	
Maximum specific growth rate, μ_{max} (h^{-1})	0.22^{b}	0.29^{b}	0.49^{a}	0.45^{a}	0.44^{a}	0.12^{b}	<0.05
Maximum biomass concentration, X_{max} (g L^{-1})	4.32^{e}	6.51^{d}	12.92^{a}	9.90^{c}	9.71^{c}	10.80^{b}	<0.05
Maximum dicoumarol activity, P_{max} (U mL^{-1})	0.02^{e}	0.10^{d}	0.349^{a}	0.285^{b}	0.231^{b}	0.221^{c}	<0.05
Final glucose concentration (g L^{-1})	0	0.1	0.2	4.9	7.86	9.25	>0.05
Amount of glucose consumed (g L^{-1})	0	4.9	9.8	10.1	12.14	15.75	>0.05
Cell efficiency, P_{max}/X_{max} (g L $cell^{-1}$)	0.004	0.015	0.027	0.028	0.024	0.019	>0.05
Overall biomass productivity, P_x (g L·h^{-1})	51.43^{cd}	90.42^{e}	153.81^{a}	117.86^{c}	134.86^{b}	150^{a}	<0.05
Overall dicoumarol productivity, $P_{dicoumarol}$ (U mL h^{-1})	1.42^{c}	3.9^{b}	4.15^{a}	3.39^{b}	3.21^{b}	3.07^{b}	<0.05
Time to reach maximum biomass, t (h)	84	72	84	84	72	72	>0.05

Note: *Means followed by the different letter in the same row of a species are significantly different at $P \leq 0.05$.

accumulation. Biomass concentration was determined by measuring biomass dry weight per L sample after 7 days of incubation period. Despite fermentation on a complex medium resulted in a greater final biomass concentration (10.21 g L^{-1}) than in a defined medium (9.33 g L^{-1}), dicoumarol production (0.214 U L^{-1}) was much lower. In contrast, the high dicoumarol production (0.322 U L^{-1}) produced in fermentation utilizing defined medium revealed that the presence of simple sugars and compounds that *A. fumigatus* can easily utilize boosted the cell build-up with a higher potential to trigger dicoumarol production.

Interestingly, while the defined medium yielded lower specific growth rate and biomass concentration values, it facilitated a higher dicoumarol concentration compared to the complex medium. This unexpected outcome implies that certain compounds or conditions within the defined medium may enhance dicoumarol production, potentially through metabolic pathways or regulatory mechanisms that are differentially influenced by the medium composition. Moreover, despite the higher dicoumarol concentration, the cell efficiency was notably higher in the defined medium, indicating a more efficient conversion of biomass into dicoumarol under its specific growth conditions. As shown in Table 1, the time required to reach maximum dicoumarol production was consistent between the two media types, suggesting that the kinetics of dicoumarol production are not significantly influenced by the type of medium used. However, the overall biomass productivity appears comparable between the two media types, indicating similar rates of biomass production despite differences in specific growth rates and biomass concentrations. These findings offer valuable insights for improving media formulations to enhance microbial performance and dicoumarol production under the most favorable conditions.

3.2. Effect of initial concentration of glucose on dicoumarol production

The performance and kinetic parameter values during fermentation of *A. fumigatus* using different concentrations of glucose was depicted in Table 2.

Specifically, variations in glucose levels markedly affect key kinetic parameters, including the specific growth rate, biomass concentration, and dicoumarol activity. Microorganisms assimilate glucose and highly favorable sugars before switching to less-favored sources of carbon such as organic acids and alcohols [35]. Consequently, a varying glucose concentration within the culture media exerts diverse effects on culture performance, influencing specific growth rate and dicoumarol productivity. The growth rate is notably low at lower glucose concentrations as shown in Table 2. Glucose concentration influences intracellular metabolites such as ATP, organic acids, and amino acids. In cultures under very glucose-limited conditions, fungal cells experience a significant reduction in ATP and amino acid concentrations, indicating an energy shortage that may limit growth rate [36].

However, in high-glucose conditions, catabolite repression may occur, whereby excess glucose represses the synthesis of enzymes involved in secondary metabolism, including those related to dicoumarol biosynthesis [37]. This repression may reduce metabolic flexibility and enzyme activity, thus lowering specific productivity despite the availability of carbon. Furthermore, accumulation of glucose metabolites may lead to feedback inhibition, disrupting key biochemical pathways essential for sustained biomass and product formation [38]. Thus, although high-glucose media in fungus cell cultures can enhance dicoumarol productivity, excessively high glucose levels may hinder cell growth. With high glucose concentration condition, cells may exhibit elevated cAMP levels, activating relevant signaling pathways of carbon metabolism [39,40] thereby reducing the specific growth rate and altering glycosylation patterns, which could be undesirable [36,41–43]. These responses suggest metabolic stress or imbalance at elevated glucose concentrations, aligning with observations of reduced growth and product yield at higher glucose levels. Dicoumarol activity, cell efficiency, and overall productivity peak at 10 g L^{-1} glucose, indicating efficient resource utilization for biomass and dicoumarol production. Deviations from this selected concentration may diminish efficiency and the overall productivity. This result not only elucidates the intricate relationship between glucose concentration and dicoumarol production kinetics in *A. fumigatus* but also indicates the fungus's sensitivity to glucose availability.

Table 3
Effect of initial concentration of nitrogen to the kinetic parameter values of dicoumarol production in submerged culture system of *A. fumigatus*.

Kinetic Parameters	Initial Concentration of Nitrogen (g L^{-1})						p-value
	0	1	2	3	4	5	
Maximum specific growth rate, μ_{max} (h^{-1})	0.04	0.05	0.10	0.15	0.12	0.11	>0.05
Maximum biomass concentration, X_{max} (g L^{-1})	0.45^{e}	4.56^{d}	8.91^{c}	9.04^{c}	10.26^{b}	11.11^{a}	<0.05
Maximum dicoumarol activity, P_{max} (U mL^{-1})	0.04^{d}	0.20^{c}	0.38^{a}	0.24^{b}	0.29^{b}	0.24^{b}	<0.05
Cell efficiency, P_{max}/X_{max} (g L $cell^{-1}$)	0.009^{d}	0.044^{a}	0.043^{a}	0.027^{b}	0.022^{c}	0.026^{b}	<0.05
Overall biomass productivity, P_x (g L h^{-1})	6.25^{e}	63.33^{d}	106.07^{cd}	107.6^{c}	122.1^{b}	132.26^{a}	<0.05
Overall dicoumarol productivity, $P_{dicoumarol}$ (U mL·h^{-1})	0.56	2.78	4.52	2.85	2.74	3.45	>0.05
Final concentration of nitrogen, (g L^{-1})	0	0	0	0	0.91	1.12	>0.05
Amount of nitrogen consumed, (g L^{-1})	0	1	2	3	3.09	3.88	>0.05
Time to reach maximum dicoumarol production, t (h)	72	72	84	84	84	84	>0.05

Note: *Means followed by the different letter in the same row of a species are significantly different at $P \leq 0.05$.

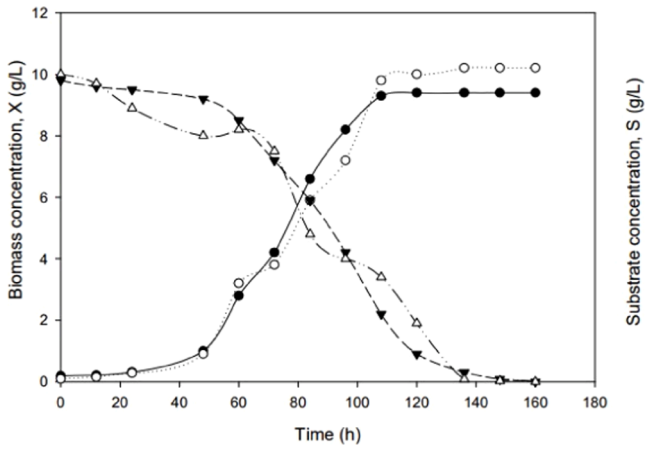

Fig. 1. Time course of batch cultivation of *A.fumigatus* in shake flask using defined medium (●); substrate (▽); biomass and complex medium (°) substrate and (▽) biomass.

3.3. Effect of initial concentration of nitrogen on dicoumarol production

The kinetic parameters from the Table 3 demonstrate the significant influence of initial concentration of nitrogen on the fermentation performance of *A. fumigatus*. Nitrogen is one of the crucial nutrient for growth, and the capacity to utilize a diverse array of nitrogen sources allows fungi to thrive in various environmental niches and endure nutrient limitations [44]. According to the findings from several researches, sodium nitrate ($NaNO_3$) is the most effective nitrogen source for *A. fumigatus*, with the highest percentage of decolorization and the best nitrogen source tested for volumetric production [45,46]. This led to our decision to use $NaNO_3$ as a nitrogen source in the present study.

Table 3 indicates that increasing $NaNO_3$ concentration resulted in a considerable increase in maximum cell concentration. However, dicoumarol synthesis was suppressed when $NaNO_3$ concentrations above 3 g L^{-1}. The maximum dicoumarol concentration (0.38 U L^{-1}) was obtained at 2 g L^{-1} of $NaNO_3$, which corresponded to the highest maximal specific growth rate and biomass concentration. Excess nitrogen availability can shift the metabolic focus of the fungus away from secondary metabolite production, such as dicoumarol, towards biomass accumulation [47]. This indicates a balance where nitrogen is sufficient to support robust fungal growth and dicoumarol biosynthesis without inducing excess cellular maintenance or inhibitory effects. However, when the initial concentration of nitrogen increased, the effectiveness of the cells to produce dicoumarol decreased, indicating that ammonium had an inhibitory effect on the formation of dicoumarol by *A. fumigatus*. The impact of initial concentration of nitrogen on secondary metabolite production is directly linked to fungal metabolism, as nitrogen availability influences the synthesis of enzymes involved in secondary metabolism. Inadequate nitrogen levels can limit growth and secondary metabolite formation [48], while excess nitrogen can lead to metabolic shifts, limiting the fungus's ability to produce secondary metabolites [49]. This finding is in agreement with Quiterio-Gutiérrez et al. [50], that claims high concentration of the carbon source and low availability of the nitrogen source are key features to enhance growth of *Aspergillus sp.*

3.4. Fermentation kinetics and modelling of A.fumigatus

3.4.1. Evaluation of cell growth kinetics

The cell growth using selected parameters; defined media was presented in Fig. 1 by plotting X (cell dry weight, g/L) versus time (min). The kinetics constant, μmax and kinetics parameter, Ks were determined on the curve fitting method of the model. The values of specific growth rate, μ was calculated according to the cell dry weight of fungal biomass concentration, X and glucose concentration as limiting substrate, S during the exponential growth phase. In shake flasks fermentation, the growth of *A.fumigatus* was very rapid, as no lag phase was observed and the growth reached stationary phase after about 110 h (refer Fig. 1). During rapid growth, glucose was consumed at a very high rate and glucose depletion was observed before the growth reached stationary phase.

Table 4
Kinetic Parameter Values for Dicoumarol Production in Shake Flask System (Highest Yield).

Kinetic parameter values	Values
Maximum specific growth rate, μ_{max} (h^{-1})	0.28
Maximum biomass concentration, X_{max} (g L^{-1})	12.93
Maximum dicoumarol concentration, P_{max} (U L^{-1})	0.474
Cell efficiency, P_{max}/X_{max} (g L $cells^{-1}$)	0.037
Cell yield, $Y_{x/s}$ (g cells glucose $^{-1}$)	0.995
Overall biomass productivity, P_x (g mL h^{-1})	4.95
Overall dicoumarol productivity, $P_{dicoumarol}$ (U mL h^{-1})	167.92
Fermentation time (h)	84

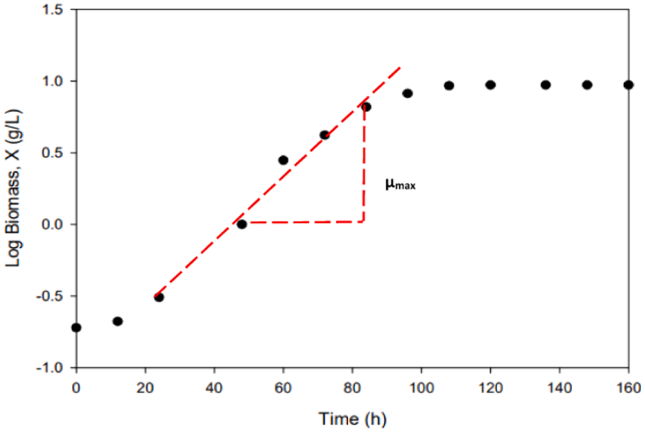

Fig. 2. Time course of log biomass for U_{max} determination.

3.4.2. Mathematical modeling

The kinetic parameter values of submerged culture system in shake flask were given in Table 4. The highest specific growth rate disclosed at 0.28 h^{-1} which corresponds to the highest rate of fungal growth achievable under ideal conditions. Accompanying this growth, the maximum biomass concentration was observed to be 12.93 g L^{-1}, signifying the maximum biomass yield attainable during fermentation. Regarding dicoumarol production, the maximum concentration reached 0.474 U L^{-1}, reflecting the highest level of dicoumarol accumulation within the fermentation medium. Additionally, the overall biomass productivity and dicoumarol productivity were determined to be 4.95 g mL h^{-1} and 167.92 U mL h^{-1}, respectively, highlighting the effectiveness of the fermentation process in producing both dicoumarol and biomass within the specified timeframe. Experimental results were used to fit the mathematical model and to calculate the kinetic parameters to reproduce the profiles of cell concentration, glucose concentration and dicoumarol production.

Experimental data (refer Table 4) was used to fit the mathematical model and calculate the kinetic parameters, allowing the prediction of the profiles for cell concentration, glucose concentration, and dicoumarol production. The values of specific growth rate (μ) were calculated based on the cell dry weight of fungal biomass (X) and glucose concentration as the limiting substrate (*S*) during the exponential growth phase. The kinetic constants, μmax (maximum specific growth rate) and Ks (Monod saturation constant), were determined by curve fitting the model to the experimental data.

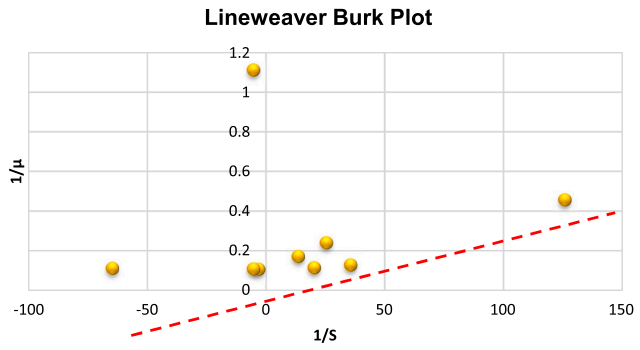

Fig. 3. Lineweaver Burk Plot for determination of Monod saturation constant.

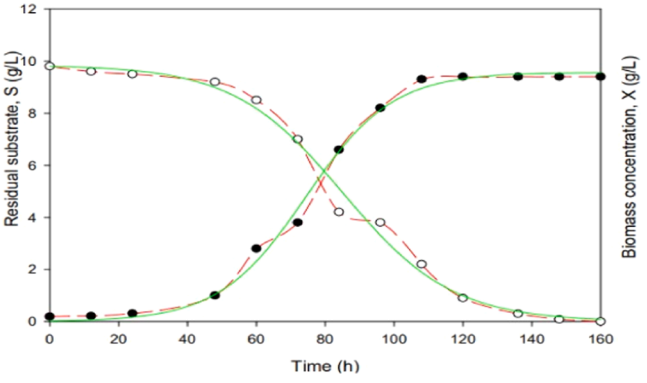

Fig. 4. Time course of batch cultivation of *A. fumigatus* in shake flask using 10g/L glucose and 2g/L $NaNO_3$ using defined medium, also showing the experimental and calculated data of biomass concentration (●); residual glucose (°) according to the proposed Monod model.

The growth of *A. fumigatus* in shake flask fermentations with defined media was presented in Fig. 1, which plots cell dry weight (X) versus time (in min). The kinetics constant, μmax, and the Monod saturation constant, Ks, were derived using curve fitting based on the experimental growth curves. The specific growth rate (μ) was determined according to the cell dry weight of fungal biomass concentration (X) and glucose concentration (S) during the exponential growth phase. The fermentation was rapid, with no lag phase observed. Growth reached a stationary phase after approximately 110 h (Fig. 1). During the rapid growth phase, glucose was consumed at a high rate, and depletion of glucose occurred before the growth reached the stationary phase.

From the data presented in Fig. 2, the maximum specific growth rate, μmax, was calculated using the following formula:

$$\mu_{max} = \frac{\ln 4.2 - \ln 0.99}{84 - 72}$$

$$\mu_{max} = 0.12h^{-1}$$

The yield on substrate ($Y_{x/s}$) was determined as:

$$Y_{x/s} = \frac{-9.3 \text{ g cells L} - 1}{(0 - 9.8) \textit{ substrate } L - 1}$$

$$= 0.95\text{g cells g substrate}^{-1}$$

To calculate the Monod saturation constant, Ks, the relationship between specific growth rate, μ, and substrate concentration, S, was determined using the Lineweaver-Burk plot, as shown in Fig. 3. The value of μmax was measured from the slope of the natural logarithm of biomass concentration (ln X) plotted against time during the log phase of growth (Fig. 2). The μmax in complex medium was approximately 45 % higher than in defined medium, suggesting that a higher μmax reduces the tendency for dicoumarol production by *A. fumigatus*.

From the Lineweaver-Burk plot, the slope $\frac{ks}{\mu max} = 0.26$

Thus, the Monod saturation constant was calculated as, $ks = 0.26 \times 0.12h^{-1} = 0.0312$ g cells substrate L^{-1}

Fig. 4 shows that the simulation curves, calculated using the Monod kinetic model, fit the experimental data from shake flask batch fermentations with more than 95 % confidence. This suggests that the Monod model is highly reliable for describing the growth of *A. fumigatus*, glucose consumption, and dicoumarol production. During the active growth phase, glucose and nitrogen were consumed to promote growth and enhance dicoumarol bioconversion. The t-test analysis revealed no significant differences at a 5 % significance level between the calculated and experimental data for cell concentration, glucose concentration, and dicoumarol synthesis in the culture (Table 2 and Table 3). This result suggests that the Monod model is sufficient for describing the key biological processes in this system.

To summarize, the Monod model provides an effective framework for simulating the growth of *A. fumigatus*, substrate consumption, and dicoumarol production under controlled conditions. The agreement between the experimental data and the model's predictions further reinforces the robustness and reliability of the Monod model for describing microbial growth in substrate-limited environments. This model is particularly useful for improving fermentation processes involving *A. fumigatus* and could potentially be scaled up for industrial applications.

3.5. Identification and characterisation of dicoumarol compound

3.5.1. Separation of dicoumarol using HPLC fractionation

The reversed-phase separation mode is commonly used for HPLC separation of mixtures of coumarin derivatives, particularly dicoumarol, which is apparent in Table 5.

In this study, the work focused on development of HPLC method for separation and determination of dicoumarol. Fig. 5 shows the comparison of chemical profiles between standards and the sample fraction with identical major peak detected at UV detection wavelength of 303 nm. The major peak was identified as dicoumarol by comparing their retention time with the standards dicoumarol which were about 2.29 min. The chromatogram of both is slightly different in which the peak of dicoumarol sample fraction was smaller compared to the standard and was proven by HPLC chromatogram as shown in Fig. 5. There is also a peak detected at the retention time of 2.78 min identified as remaining o-coumaric acid.

Table 5
The highest peaks of theoretical and experimental precursor ion by tandem mass spectrum.

Sample	Theoretical precursor ion m/z (±2 Da)	Experimental precursor ion m/z (±2 Da)	Theoretical product ion m/z (±2 Da)	Experimental product ion m/z (±2 Da)
Standard	336.063	338.919	NA	NA
			81.000	81.092
			139.200	139.00
Sample Fraction	336.063	336.965	199.000	196.950
			257.200	254.800
			335.000	336.965

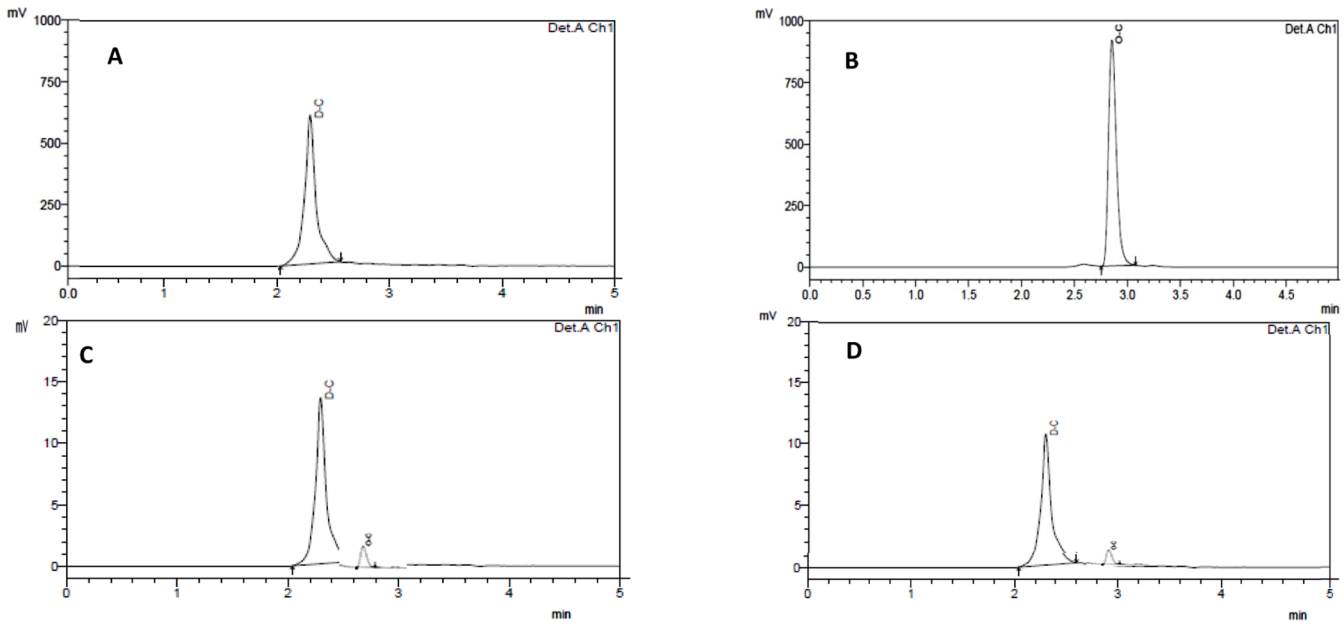

Fig. 5. Chromatogram of dicoumarol using HPLC fractionation method (A) dicoumarol standard; (B) o-coumaric acid standard; (C) sample fraction of dicoumarol in defined medium and (D) sample fraction in complex medium with methanol-acetic acid mobile phase composition at 303 nm of wavelength.

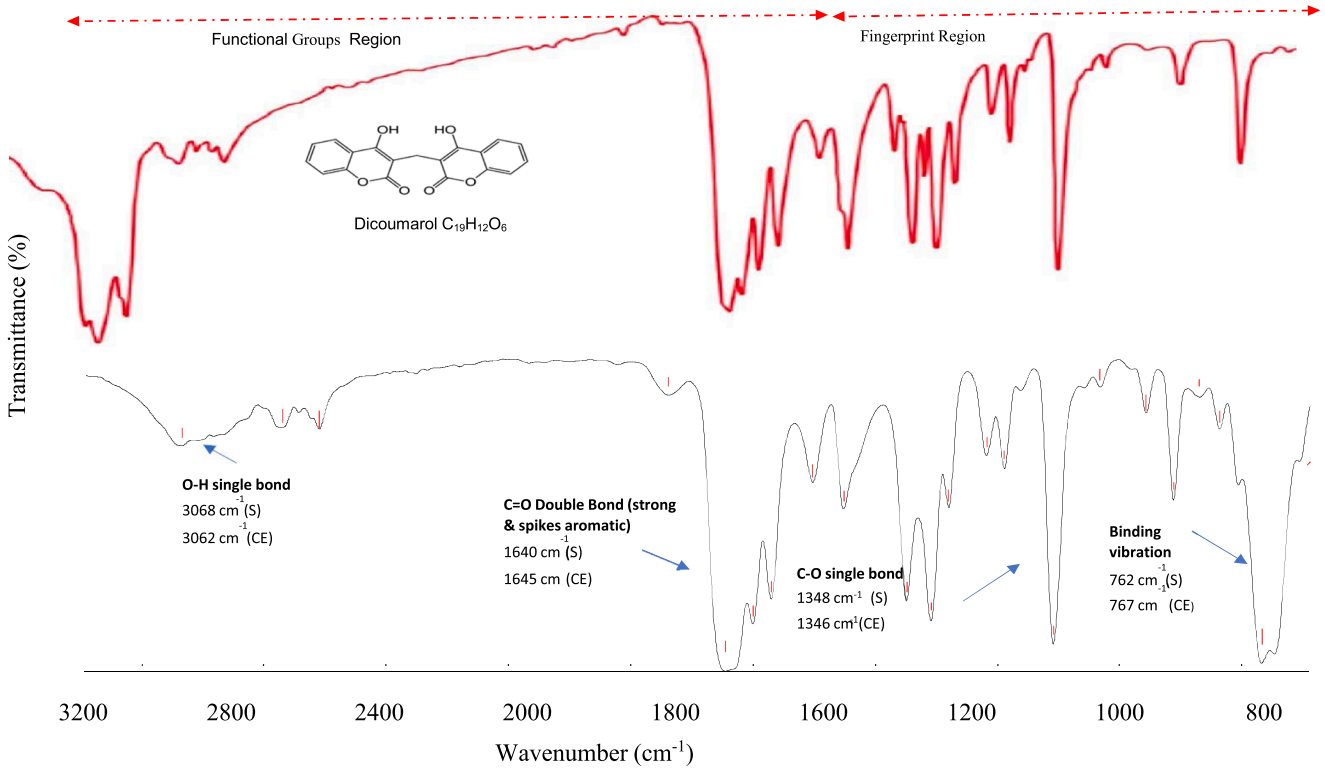

Fig. 6. Experimental FT-IR spectra of dicoumarol comparing standard (red lines) and sample fraction (black lines).

The amounts of dicoumarol sample fraction were calculated from the peak area by using the calibration curves developed from the standards as the control in the analysis. The results showed that the concentration of dicoumarol in the sample fraction was identical to the standard, with both exhibiting the same retention time, further confirming the identity of the compound. This result not only verifies that the sample fraction contained dicoumarol but also demonstrates the reliability of the extraction methods used by our previous study [11]. The recovery rate for dicoumarol was found to be 90 % following the extraction and purification process for the 60-ppm solution, indicating high efficiency of the method. The recovery value suggests that minimal loss of dicoumarol occurred during the extraction process, ensuring the integrity of the sample. These findings are also consistent with similar studies in the literature, including a study by Hroboňová,et al. [51], where dicoumarol recovery in sweet clover was reported to range from 88.6 % to 92.6 % using HPLC-DAD analysis. This consistency further supports the effectiveness of the analytical approach employed in this study for quantifying dicoumarol and highlights the robustness of the method in

Table 6
Surface chemistry for sample fraction of dicoumarol.

Bond Type	Functional Group/ Wavelength
O-H single bond	• Based on the spectra of the dicoumarol standard, there is a broad and intense -OH single bond stretching frequencies at the range of 3000-3200 cm^{-1}
C-H stretching frequencies	• At the region of C-H stretching frequencies, there are two or three bands of weak to medium intensity have been observed at the region of 2618 to 2735 cm-1. These absorptions were due to the C-H stretching vibrations of the pyrene, benzene and furan rings.
C=O double bond	• The C=O stretching frequency of dicoumarol is usually observed at the region 1700 to 1750 cm-1 whereas in chromones (γ-pyrones) it was found at ~1650 cm-1. The 6-O and 7-O- coumarin glycosides have their C=O frequencies below 1700cm-1. • Infrared spectrum reveals absorption bands around 1737 cm−1 which was assigned to the C=O stretching frequency of the ketone. The standard spectra of dicoumarol showed as strong C=O absorption at 1660 to 1680 cm-1. This was presumably due to the intramolecular hydrogen bond between the 2'-hydroxyl and pyrone-carbonyl groups. The low C=O frequency (1660cm-1) of dicoumarol was also revealed to have the strong intramolecular hyrodgen bonding between the two halves of the molecules. • Normally, there were three absorption bands at the region of 1600 to 1660 cm-1 in the standard spectra of dicoumarol. This pattern of absorption provides a quick method of differentiation from isomeric chromones in which the absorption is generally much simpler. • There is an addition to the aromatic bands at ~1500 and ~1600 cm-1, a strong sharp band appears at 1645 cm-1 which was attributed to the C=C stretching of the furan ring.
C=C skeletal vibrations	• Dicoumarol's infrared spectra typically showed three absorption bands range in 1600–1660 cm^{-1}. This absorption pattern allows for easy distinction from isomeric chromones, which absorption is typically less complex. • A strong, sharp band appearing at 1645 cm^{-1} and is associated with the C=C stretching of the furan ring, as well as aromatic bands at about 1500 and 1600 cm^{-1}.
Other bands	• Bands at 1088 to 1109 and 1253 to 1274 cm^{-1} in the dicoumarol spectra were considered to be characteristics of C-O stretching of the furan group. • Owing to in-plane and out-of-plane deformations of the furan C-H bonds, there are bands at the 710 to 767 and 826 to 869 cm^{-1}, respectively. • Absorption bands at around 1737 cm^{-1} correspond to the ketone's C=O stretching frequency. • The lactone ring's C-O stretching frequency was allocated to a weak band that ranged between 1031 and 1188 cm^{-1}. • Both compounds exhibited a strong vibration at around 1108 cm^{-1}, which was attributed to the corresponding band for the ketone C=O carbon.

extracting and analyzing the compound from complex samples.

3.5.2. Characterisation of dicoumarol using FT-IR spectra

The determination and identification of the functional groups of the converted sample of dicoumarol were then confirmed through the infrared spectroscopy by superimposing its spectra with the standard. Based on Fig. 6 and Table 6, dicoumarol structure ($C_{19}H_{12}O_6$) was spread by the FT-IR spectra on the following grounds;

3.5.3. Characterisation of dicoumarol using liquid chromatography mass spectrometry

The structure of dicoumarol was confirmed and quantified using LC-MS/MS with Electron Impact (EI) mode, which facilitated the generation of a distinct fragmentation pattern essential for its identification. In the mass spectrum, the X-axis represents the m/z ratio, indicating the mass-to-charge ratio, while the Y-axis shows intensity, reflecting the ion abundance detected by the mass spectrometer. As depicted in Fig. 7, four daughter ion spectra of dicoumarol were produced through collision-activated dissociation (CAD) at a collision offset of –10 V from the 70-eV EI, with the parent ion (M+) observed at m/z 336. The characteristic EI daughter ions were detected at m/z 257.2, 199.0, 139.2, and 81 in the dicoumarol standard, and at m/z 254.8, 196.95, 139.0, and 81.09 in the sample fraction (Fig. 7). The product ion at 254 m/z for sample fraction likely results from the loss of a neutral group, such as a methyl or amide group, which aligns with common fragmentation pathways observed in aromatic and heterocyclic compounds, as reported in Uchiyama et al. [52]. The product ion at 139 m/z in sample fraction aligns with common fragmentation patterns in aromatic compounds, as observed in catechins, which are known for their antioxidant properties [53]. This highlights the consistency of fragmentation pathways for aromatic compounds in mass spectrometry, further supporting the robustness of the observed fragmentation in dicoumarol. Additionally, the peak scan of molecular ion of 336.8 m/z concluded that the sample fraction was successfully identified as dicoumarol. This finding is equivalent to the one investigated by Fourel et al. [54] which also found that determination among 14 anticoagulant rodenticides, dicoumarol gave 335.0 m/z of precursor ion at 7 min of retention time.

3.6. In vitro rodenticide anticoagulant activity

Dicoumarol served as the positive control, demonstrating significant anticoagulant activity with a prothrombin time (PT) exceeding 60 seconds, compared to the negative control at 19.07 ± 0.32 s. In the aPTT test, dicoumarol showed a prolonged coagulation time greater than 120 seconds, while the negative control remained at 30.26 ± 0.03 s. As illustrated in Fig. 8, the dicoumarol fraction extended the coagulation time in the aPTT test by more than twice the time observed for the dry extract, emphasizing its potent anticoagulant effect. Notably, no significant prolongation was seen in the PT test. The prolonged aPTT suggests the inhibition of the intrinsic pathway of coagulation, with minimal impact on the extrinsic pathway [55,56]. These findings confirm the preferential inhibition of the intrinsic coagulation pathway by the dicoumarol fraction. Moreover, while dicoumarol remains the primary contributor to the observed anticoagulation enhancement, o-coumaric acid also demonstrates anticoagulant activity. It appears that o-coumaric acid could offer a more sustainable anticoagulation effect, with a consistent therapeutic profile and potentially fewer side effects, making it a promising candidate for clinical applications.

4. Conclusion

In conclusion, this study highlights the significant impact of fermentation conditions on the bioconversion of dicoumarol using o-coumaric acid extracted from *G.sepium* leaves by *A. fumigatus*. Using a defined medium, with 10 g L^{-1} glucose and 2 g L^{-1} $NaNO_3$, the fermentation process achieved the highest dicoumarol productivity of 153.81 U $mL\ h^{-1}$, along with increased cell efficiency (0.027 g L $cell^{-1}$) and dicoumarol yield (4.15 U $mL{\cdot}h^{-1}$), highlighting the effectiveness of these conditions for enhanced production. The highest dicoumarol production (0.322 U L^{-1}) achieved with the modified medium underscores the value of incorporating simple sugars and easily utilized compounds, which promote cell growth and enhance dicoumarol production. The kinetics of dicoumarol production were accurately modeled using the Monod equation, providing valuable insights into microbial growth, substrate consumption, and dicoumarol biosynthesis during batch fermentation. The Monod model proved effective in simulating the relationship between growth rate, substrate concentration, and biomass production, offering a reliable framework for enhancing fermentation conditions. Additionally, the identification of dicoumarol through HPLC analysis, coupled with its confirmed anticoagulant activity in aPTT tests, emphasizes its pharmaceutical potential. The LCMS/MS analysis further validated the successful conversion of o-coumaric acid from *G. sepium* leaves into dicoumarol, showcasing the scalability and sustainability of this bioconversion process. Despite these promising results, further

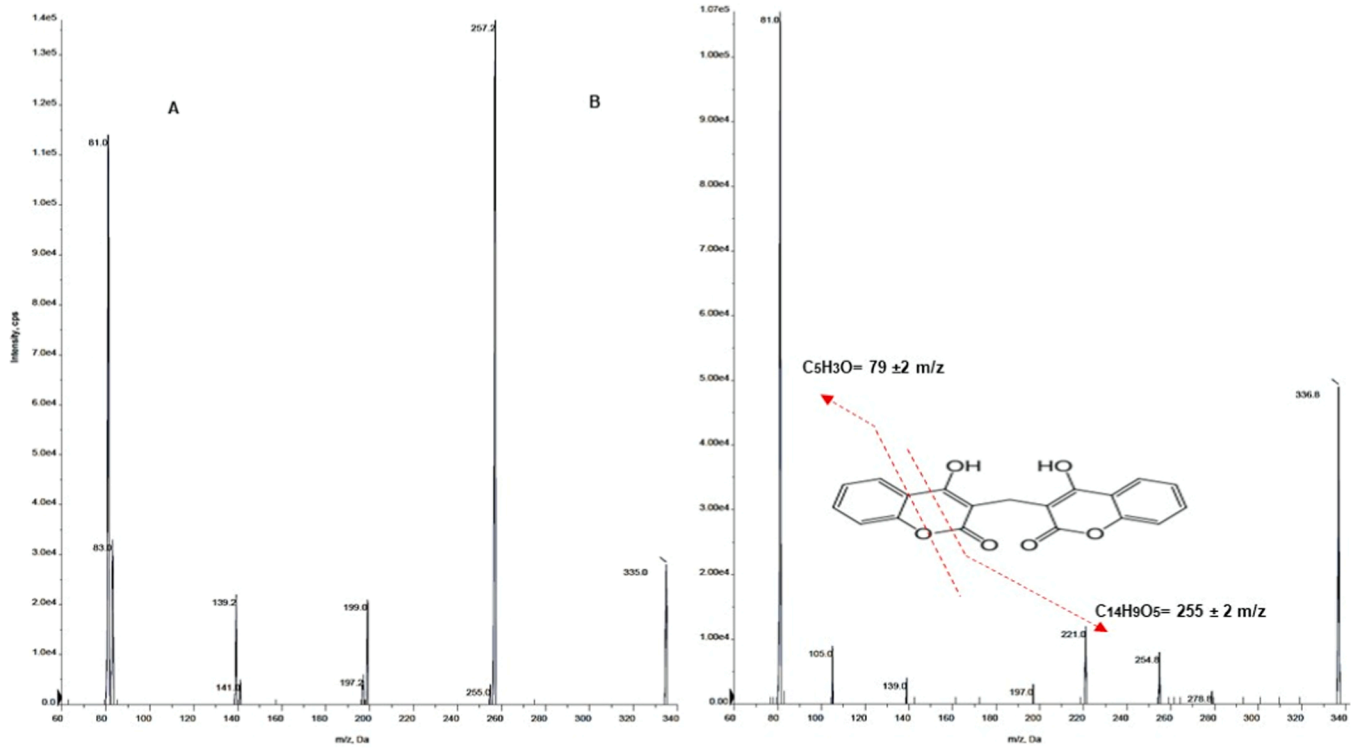

Fig. 7. LC MS/MS positive EI (70 eV) daughter ion spectrum resulting from argon collision activated dissociation at a collision offset of – 10 V (A) standard; (B) sample fraction.

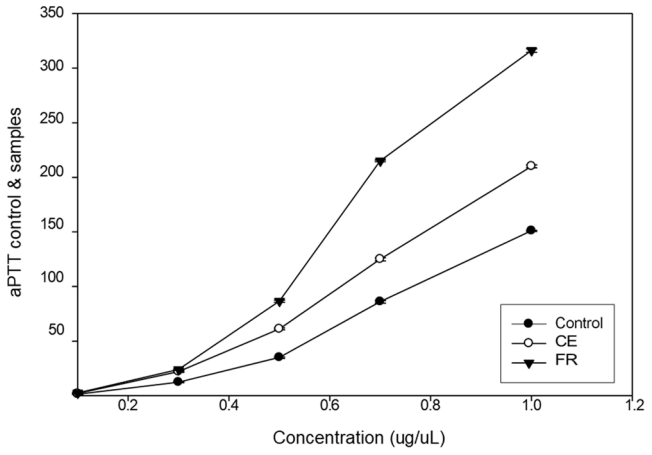

Fig. 8. Activated Partial Thromboplastin Time for dicoumarol; control, dry extract (DE) and dicoumarol fraction (FR).

studies are needed to investigate the long-term stability of the fermentation process and the optimization of nutrient ratios to further enhance productivity. Additionally, exploring larger-scale fermentation systems will be essential for confirming the industrial applicability of this method. Overall, this research lays a strong foundation for the sustainable and scalable production of dicoumarol, with potential applications in the pharmaceutical and medical industries.

CRediT authorship contribution statement

Siti Zalina Yaacob: Writing – original draft, Methodology, Investigation, Data curation, Conceptualization. **Luqman Chuah Abdullah:** Visualization, Supervision, Resources, Project administration, Funding acquisition. **Chuan Li Lee:** Writing – review & editing, Visualization, Methodology, Formal analysis, Data curation. **Nor Hafizah Abdullah:** Validation, Supervision. **Kit Ling Chin:** Writing – review & editing, Validation, Formal analysis, Data curation.

Declaration of competing interest

The authors declare that they have no known competing financial interests or personal relationships that could have appeared to influence the work reported in this paper.

Acknowledgement

The authors would like to acknowledge all of the laboratory workers at Universiti Putra Malaysia's Department of Chemical and Environmental Engineering for their assistance with this research.

Data availability

The data that has been used is confidential.

References

[1] V.L.M. Silva, et al., Dicoumarol: from chemistry to antitumor benefits, Chin. Med. (U. K.) 17 (145) (2022) 1–20, https://doi.org/10.1186/s13020-022-00699-0.
[2] K. Rashed, Biological evidences of dicoumarol: A review, Plantae Sci. 4 (2) (2021) 121–124, https://doi.org/10.32439/ps.v4i2.121-124.
[3] C. Sun, W. Zhao, X. Wang, Y. Sun, X. Chen, A pharmacological review of dicoumarol: an old natural anticoagulant agent, Pharmacol. Res. 160 (2020) 105193, https://doi.org/10.1016/j.phrs.2020.105193.
[4] Y. Peng, et al., Dicoumarol is an effective post-exposure prophylactic for SARS-CoV-2 Omicron infection in human airway epithelium, Signal Transduct. Target. Ther. 8 (1) (2023), https://doi.org/10.1038/s41392-023-01511-7.
[5] A. Mnasri, N. Amri, H. Ghalla, R. Gatri, N. Hamdi, Effective synthesis and biological evaluation of dicoumarols: preparation, characterization, and docking studies, ACS Omega 8 (17) (2023) 14926–14943, https://doi.org/10.1021/acsomega.2c06802.
[6] Z. Wu, P. Huang, Q. Wang, J. Li, Z. Sun, H. Li, Coumarin-monoterpenes from *Gerbera anandria* (Linn.) Sch.-bip and their neuroprotective activity, Bioorg. Chem. 124 (2022) 105826.

[7] O. Morebise, Medicinal plants of Dominica-uses, chemical constituents, bioactivities and prospects, J. Med. Plants Stud. 3 (5) (2015) 144–154.

[8] F. He, M. Wang, M. Gao, M. Zhao, Y. Bai, C. Zhao, Chemical composition and biological activities of Gerbera anandria, Molecules 19 (4) (2014) 4046–4057, https://doi.org/10.3390/molecules19044046.

[9] Y. Zou, Y. Teng, J. Li, Y. Yan, Recent advances in the biosynthesis of coumarin and its derivatives, Green Chem. Eng. 5 (2) (2024) 150–154, https://doi.org/10.1016/j.gce.2023.04.003.

[10] T. Takemura, T. Kamo, E. Sakuno, S. Hiradate, Y. Fujii, Discovery of coumarin as the predominant allelochemical in *Guricidia sepium*, J. Trop. For. Sci. 25 (2) (2013) 268–272.

[11] S.Z. Yaacob, L.C. Abdullah, N. Abdullah, C.L. Lee, K. Ling, H. Xiao, Extraction process of o-coumaric acid from *Gliricidia sepium* leaves : optimization and kinetic studies, J. Adv. Res. Micro Nano Eng 30 (1) (2025) 58–80.

[12] P. Ejigboye, et al., Anaerobic digestion of *Gliricidia sepium* inoculated with pig dung using a portable bio-digester for process optimization, Results Eng 25 (2025) 103550, https://doi.org/10.1016/j.rineng.2024.103550.

[13] B. Jin, X. Xu, Wholesale price forecasts of green grams using the neural network, Asian J. Econ. Bank (2024), https://doi.org/10.1108/ajeb-01-2024-0007.

[14] B. Jin, X. Xu, Machine learning coffee price predictions, Eng. Econ. 17 (04) (2025) 1–27, https://doi.org/10.1080/0013791X.2025.2464130.

[15] A. Zulaika, H. Rahman, S.S. Ningrum, A.F. Maulida, Exploring microbial lipases: screening and identification for biocatalyst potential in bioethanol synthesis from glycerol-based biodiesel waste, Results Eng. 23 (2024) 102427, https://doi.org/10.1016/j.rineng.2024.102427.

[16] M.G. Hassan, et al., Anti-cancer and anti-oxidant bioactive metabolites from *Aspergillus fumigatus* WA7S6 isolated from marine sources: In vitro and in silico studies, Microorganisms 12 (2024) 127, https://doi.org/10.3390/microorganisms12010127.

[17] Z. Octarya, R. Novianty, N. Suraya, Saryono, Antimicrobial activity and GC-MS analysis of bioactive constituents of *Aspergillus fumigatus* 269 isolated from Sungai Pinang hot spring, Riau, Indonesia, Biodiversitas 22 (4) (2021) 1839–1845, https://doi.org/10.13057/biodiv/d220429.

[18] N.K. Borah, Y. Tripathi, A. Parashar, S. Santoshi, H. Bansal, A comprehensive and intricate dynamics of *Aspergillus*: implications, therapeutic challenges, and drug resistance. Recent Advances in Human Fungal Diseases: Progress and Prospects, Springer Nature Singapore, Singapore, 2024, pp. 427–455.

[19] R. Orfali, et al., Recent updates on the bioactive compounds of the marine-derived genus Aspergillus, 11, Royal Society of Chemistry, 2021, https://doi.org/10.1039/d1ra01359a.

[20] S. Krappmann, G.H. Braus, Nitrogen metabolism of *Aspergillus* and its role in pathogenicity, Med. Mycol 43 (2005) 31–40, https://doi.org/10.1080/13693780400024271.

[21] Z.H. Wardah, H.G. Chaudhari, V. Prajapati, G.G. Raol, Application of statistical methodology for the optimization of l-glutaminase enzyme production from *Streptomyces pseudogriseolus* ZHG20 under solid-state fermentation, J. Genet. Eng. Biotechnol. 21 (2023) 138, https://doi.org/10.1186/s43141-023-00618-2.

[22] R. Kembaren, et al., Optimization of erythritol production through fermentation using molasses as carbon source, Acta Biochim. Pol 71 (2025) 14000, https://doi.org/10.3389/ABP.2024.14000.

[23] R. Bhaturiwala, M. Bagban, A. Mansuri, H. Modi, Successive approach of medium optimization using one-factor-at-a-time and response surface methodology for improved β-mannanase production from *Streptomyces sp*, Bioresour. Technol. Rep. 18 (May) (2022) 101087, https://doi.org/10.1016/j.biteb.2022.101087.

[24] S.K. Gupta, S. Sundar, Kinetics of microbial growth, substrate consumption, and product formation. Recent Advances in Bioprocess Engineering and Bioreactor Design, Springer Nature Singapore, Singapore, 2024, pp. 75–114, https://doi.org/10.1016/0022-5193(63)90058-4.

[25] I.Nor Faekah, S. Fatihah, Z.S. Mohamed, Kinetic evaluation of a partially packed upflow anaerobic fixed film reactor treating low-strength synthetic rubber wastewater, Heliyon 6 (2020) e03594, https://doi.org/10.1016/j.heliyon.2020.e03594.

[26] M. Muloiwa, S. Nyende-Byakika, M. Dinka, Comparison of unstructured kinetic bacterial growth models, S. Afr. J. Chem. Eng 33 (2020) 141–150, https://doi.org/10.1016/j.sajce.2020.07.006.

[27] R.L. Wang, M.J. Li, The study of novelty nutrients supplementary scheme and methodology on advanced carbon sequestration of microalgae, Results Eng. 22 (2024) 102178, https://doi.org/10.1016/j.rineng.2024.102178.

[28] K. Hroboňová, A. Machyňáková, J. Čižmárik, Determination of dicoumarol in *Melilotus officinalis* L. by using molecularly imprinted polymer solid-phase extraction coupled with high performance liquid chromatography, J. Chromatogr. A 1539 (2018) 93–102, https://doi.org/10.1016/j.chroma.2018.01.043.

[29] C.L. Lee, K.L. Chin, P.S. H'ng, M.S. Hafizuddin, P.S. Khoo, Valorisation of underutilized grass fibre (stem) as a potential material for paper production, Polym. 14 (23) (2022) 5203, https://doi.org/10.3390/polym14235203.

[30] S. Lu, X. Sun, Y. Zhang, Insight into metabolism of CHO cells at low glucose concentration on the basis of the determination of intracellular metabolites, Process Biochem 40 (5) (2005) 1917–1921, https://doi.org/10.1016/j.procbio.2004.07.004.

[31] A.L. Guedes, L.M. Casanova, M.N. Coelho, F.S. Frattani, S.S. Costa, R.B. Zingali, Anti-hemostatic, antithrombotic, and chemical profiles of a curly-leaf variety of *Petroselinum crispum* (Apiaceae), a food and medicinal aromatic herb, Fitoterapia 175 (2024) 105894, https://doi.org/10.1016/j.fitote.2024.105894.

[32] J. Félix-Silva, et al., In vitro anticoagulant and antioxidant activities of *Jatropha gossypiifolia* L. (Euphorbiaceae) leaves aiming therapeutical applications, BMC Complement. Altern. Med 14 (2014) 405, https://doi.org/10.1186/1472-6882-14-405.

[33] K.R. Westphal, et al., The effects of different potato dextrose agar media on secondary metabolite production in Fusarium, Int. J. Food Microbiol 347 (2021) 109171, https://doi.org/10.1016/j.ijfoodmicro.2021.109171.

[34] N. Jahan, S. Sultana, S.K. Adhikary, S. Rahman, S. Yasmin, Evaluation of the growth performance of *Trichoderma harzianum* (Rifai.) on different culture media, IOSR J. Agric. Vet. Sci 3 (4) (2013) 44–50, https://doi.org/10.9790/2380-0344450.

[35] M. Adnan, et al., Carbon catabolite repression in filamentous Fungi, Int. J. Mol. Sci 19 (2018) 1–23, https://doi.org/10.3390/ijms19010048.

[36] S. Lu, X. Sun, Y. Zhang, Insight into metabolism of CHO cells at low glucose concentration on the basis of the determination of intracellular metabolites, Process Biochem 40 (2005) 1917–1921, https://doi.org/10.1016/j.procbio.2004.07.004.

[37] A. Romero-Rodríguez, B. Ruiz-Villafán, V.H. Tierrafría, R. Rodríguez-Sanoja, S. Sánchez, Carbon catabolite regulation of secondary metabolite formation and morphological differentiation in *Streptomyces coelicolor*, Appl. Biochem. Biotechnol. 180 (6) (2016) 1152–1166, https://doi.org/10.1007/s12010-016-2158-9.

[38] H. Sun, W. Zhao, X. Mao, Y. Li, T. Wu, F. Chen, High-value biomass from microalgae production platforms: strategies and progress based on carbon metabolism and energy conversion, Biotechnol. Biofuels 11 (1) (2018) 1–23, https://doi.org/10.1186/s13068-018-1225-6.

[39] M. Vergara, et al., High glucose and low specific cell growth but not mild hypothermia improve specific r-protein productivity in chemostat culture of CHO cells, PLoS One 13 (8) (2018) 1–22, https://doi.org/10.1371/journal.pone.0202098.

[40] H.H. Lin, T.Y. Lee, T.W. Liu, C.P. Tseng, High glucose enhances cAMP level and extracellular signal-regulated kinase phosphorylation in Chinese hamster ovary cell: usage of Br-cAMP in foreign protein β-galactosidase expression, J. Biosci. Bioeng 124 (1) (2017) 108–114, https://doi.org/10.1016/j.jbiosc.2017.02.010.

[41] Z. Liu, et al., A quantitative proteomic analysis of cellular responses to high glucose media in Chinese hamster ovary cells, Biotechnol. Prog 31 (4) (2015) 1026–1038, https://doi.org/10.1002/btpr.2090.

[42] I.H. Yuk, et al., Controlling glycation of recombinant antibody in fed-batch cell cultures, Biotechnol. Bioeng 108 (11) (2011) 2600–2610, https://doi.org/10.1002/bit.23218.

[43] D. Reinhart, L. Damjanovic, C. Kaisermayer, R. Kunert, Benchmarking of commercially available CHO cell culture media for antibody production, Appl. Microbiol. Biotechnol 99 (11) (2015) 4645–4657, https://doi.org/10.1007/s00253-015-6514-4.

[44] B. Tudzynski, Nitrogen regulation of fungal secondary metabolism in fungi, Front. Microbiol 5 (2014) 1–15, https://doi.org/10.3389/fmicb.2014.00656.

[45] W. Yang, W.S. Kim, A. Fang, A.L. Demain, Carbon and nitrogen source nutrition of fumagillin biosynthesis by *Aspergillus fumigatus*, Curr. Microbiol. 46 (4) (2003) 275–279, https://doi.org/10.1007/s00284-002-3842-2.

[46] M. Pazouki, N.A. Hossein, F.M. Bani, J. Shaigan, Decolorization of distillery wastewater by dv irradiated spores of *Aspergillus Fumigatus*, Iranuan J. Chem. Eng. 2 (2) (2005) 49–55.

[47] Y. Bao, et al., Integration of transcriptomic and metabolomic profiles provides insights into the influence of nitrogen on secondary metabolism in *Fusarium sacchari*, Int. J. Mol. Sci. 24 (2023) 10832, https://doi.org/10.3390/ijms241310832.

[48] M.H. Ibrahim, H.Z.E. Jaafar, A. Rahmat, Z.A. Rahman, Effects of nitrogen fertilization on synthesis of primary and secondary metabolites in three varieties of kacip fatimah (*Labisia pumila* blume), Int. J. Mol. Sci. 12 (8) (2011) 5238–5254, https://doi.org/10.3390/ijms12085238.

[49] S. Sanchez, A.L. Demain, Metabolic regulation and overproduction of primary metabolites, Microb. Biotechnol. 1 (4) (2008) 283–319, https://doi.org/10.1111/j.1751-7915.2007.00015.x.

[50] T. Quiterio-Gutiérrez, et al., Production of kojic acid by *Aspergillus niger* M4 with different concentrations of yeast extract as a nitrogen source, Processes 11 (6) (2023) 1724, https://doi.org/10.3390/pr11061724.

[51] K. Hroboňová, J. Sádecká, J. Čižmárik, HPLC separation and determination of dicoumarol and other simple coumarins in sweet clover, Nov. Biotechnol. Chim. 17 (1) (2018) 95–102, https://doi.org/10.2478/nbec-2018-0010.

[52] M. Uchiyama, et al., Identification of novel metabolic pathways of pioglitazone in hepatocytes: N-glucuronidation of thiazolidinedione ring and sequential ring-opening pathway, Drug Metab. Dispos. 38 (6) (2010) 946–956, https://doi.org/10.1124/dmd.109.031583.

[53] Z. Spáčil, L. Nováková, P. Solich, Comparison of positive and negative ion detection of tea catechins using tandem mass spectrometry and ultra high performance liquid chromatography, Food Chem. 123 (2) (2010) 535–541, https://doi.org/10.1016/j.foodchem.2010.04.048.

[54] I. Fourel, C. Hugnet, I. Goy-Thollot, P. Berny, Validation of a new liquid chromatography-tandem mass spectrometry ion-trap technique for the simultaneous determination of thirteen anticoagulant rodenticides, drugs, or natural products, J. Anal. Toxicol 34 (2) (2010) 95–102, https://doi.org/10.1093/jat/34.2.95.

[55] W. Mao, et al., Chemical characteristic and anticoagulant activity of the sulfated polysaccharide isolated from *Monostroma latissimum* (Chlorophyta), Int. J. Biol. Macromol. 44 (2009) 70–74, https://doi.org/10.1016/j.ijbiomac.2008.10.003.

[56] A.F.D. Vasconcelos, et al., Sulfonation and anticoagulant activity of fungal exocellular β-(1→6)-d-glucan (lasiodiplodan), Carbohydr. Polym 92 (2013) 1908–1914, https://doi.org/10.1016/j.carbpol.2012.10.034.